ISTITUTO NAZIONALE DI FISICA NUCLEARE

Sezione di Perugia

INFN/AE–96/42
17 Dicembre 1996

A. Codino and M. Lanfranchi:

OPTIMUM RIGIDITY RANGE FOR THE COSMIC ANTIHELIUM QUEST

SIS–Pubblicazioni
dei Laboratori Nazionali di Frascati

INFN – Istituto Nazionale di Fisica Nucelare
Sezione di Perugia

INFN/AE–96/42
17 Dicembre 1996

OPTIMUM RIGIDITY RANGE FOR THE COSMIC ANTIHELIUM QUEST

A. Codino and M. Lanfranchi

Dipartimento di Fisica dell'Università di Perugia

and

Istituto Nazionale di Fisica Nucleare (INFN), Italy

Abstract

No cosmic antinucleus has yet been detected in the primary cosmic radiation. Only upper limits to the antinucleus fluxes have been measured in various rigidity ranges in different experiments. Calculations of the flux reduction experienced by cosmic antihelium traversing the Milky Way are reported. A significant depression of the antihelium flux has been found in the low momentum band 2 - 6 GeV/c compared to that postulated to exist in the intergalactic space. The relevant results presented here are based on simple observational data regarding the total matter column swept by cosmic rays in the Milky Way and the expected properties of antihelium interactions with the interstellar hydrogen. The calculations have been made by the simulation code LEASA (Low Energy Antinucleus Simulation Algorithms) developed to describe antinucleus interactions with matter. Implications of these results on past and future experiments giving

1 Introduction

Many experiments have been performed (Aizu et al. 1961; Grigorov et al. 1964; Ivanova et al. 1968; Greenhil et al. 1971; Evenson et al. 1972; Verma et al. 1973; Golden et al. 1974; Smoot et al. 1975; Badhwar et al. 1978; Buffington et al. 1981; Lund and Rotenberg 1986; Ormes et al. 1995) or only proposed (Codino et al. 1994; Balebanov et al. 1995) to determine a finite flux of antinuclei in the primary cosmic radiation. The existence of antinuclei is predicted by symmetric theories of the Universe which contemplate equal amounts of macroscopic matter and antimatter separated by an unknown, critical distance to impede global annihilation. Antimatter conglomerates are expected to be made of antistars, antigalaxies and other hypothetical celestial bodies made of bound systems of antinuclei and orbital positrons. Upper limits to the antinucleus-nucleus flux ratios of all experiments made since 1961 are shown in table 1. New experiments with enhanced sensitivity are in preparation.

Note that the negative outcomes of antinucleus searches may be regarded as a reinforcement of standard cosmology. Absence of antinuclei in the cosmic radiation, eventually established with a sensitivity greater than that already measured, would complement other overwhelming observational evidence (the linear recession velocity of galaxies versus distance, the existence of cosmic background radiation, the relative abundances of light elements, etc.) that supports standard cosmology.

From the nuclear theory of stellar evolution applied to antihydrogen and light antinuclei, it may be conjectured that heavy antinuclei are synthetized in antistars. Thus, in this hypothesis, antinuclei are a fingerprint of the existence of antistars, antigalaxies and antimatter conglomerates. In fact, due to the small probability of occurrence, antinuclei cannot be produced by hadronic interactions of ordinary cosmic rays with ambient matter. Antinuclei of the cosmic radiation leaked out from antigalaxies may reach large distances and signal the existence of macroscopic antimatter conglomerates. Antihelium out of other antinuclides of the cosmic radiation coming from antigalaxies is believed to be the most abundant species besides antiprotons. Heavier antinuclei in the cosmic radiation are predominantly destroyed by nuclear interactions which, in turn, can produce antihelium and other fragments. Antiprotons are the most abundant species of cosmic rays expected to be produced in antigalaxies as protons are in galaxies. However, the

Table 1: Upper limits to the antinucleus-nucleus flux ratios in the primary cosmic radiation determined by cosmic ray experiments in the period 1961-1995.

Atomic Number $\|Z\|$	Rigidity range (GV/c)	Number of events	Upper limits on the flux ratios	Experiment
2	$1.3 - 2.7$	500	7×10^{-3}	Aizu et al. (1961)
	1.2-10.4	2189	1.4×10^{-3}	Evenson (1972)
	10-25	40	8×10^{-2}	Evenson (1972)
	$14 - 100$	116	10^{-2}	Verma et al. (1973)
	4-33	6300	5×10^{-4}	Smoot et al. (1975)
	33-100	180	2×10^{-2}	Smoot et al. (1975)
	4-33	$2.3\ 10^4$	10^{-4}	Badhwar et al. (1978)
	33-100	100	10^{-2}	Badhwar et al. (1978)
	< 0.2	10^5	3×10^{-5}	Buffington et al. (1981)
	$1 - 1.8$	1.5×10^5	2.2×10^{-5}	Buffington et al. (1981)
	$1 - 19$	11.43×10^5	8×10^{-6}	Ormes et al. (1995)
≥ 3	< 3	-	2×10^{-2}	Grigorov et al. (1964)
	< 4	-	2×10^{-2}	Ivanova et al. (1968)
	4-125	416	5×10^{-3}	Golden et al. (1974)
	4-33	4.1×10^4	8×10^{-5}	Smoot et al. (1975)
	3-100	560	6×10^{-3}	Smoot et al. (1975)
≥ 6	$1.3 - 2.7$	300	10^{-2}	Aizu et al. (1961)
	10-18	40	7×10^{-2}	Greenhill et al. (1971)
≥ 9	2-20	2.04×10^4	1.5×10^{-4}	Lund and Rotenberg (198

secondary production of antiprotons in ordinary cosmic ray collisions with ambient matter might obscure the primary production in antigalaxies. For these reasons, the quest for antinuclei in the cosmic radiation made in many experiments focuses on antihelium.

Instruments for antihelium detection should be positioned at the top of the atmosphere, on the Moon or on other sites devoid of matter to prevent antihelium interactions before detection. Antialfas, that are presumed to populate intergalactic space, should penetrate the halo of the Milky Way, then intercept the disk boundary and finally enter the solar cavity where the detector is located. A schematic illustration of an antihelium trajectory intercepting the galactic cavity is displayed in figure 1. In analogy to the solar cavity, we use the term galactic cavity to denote that space region occupied by the Milky Way. The magnetic field strength and the cosmic ray density in the galactic cavity differ by at least one order of magnitude from those of the intergalactic space surrounding the Galaxy.

Extragalactic antihelium arriving close to the Earth will experience ionization energy losses and nuclear interactions in the interstellar medium. As a result of these interactions low energy antialfas will never reach the solar cavity, implying a low energy cutoff in the antihelium energy spectrum. The main purpose of this paper is to determine the antihelium rigidity cutoff and to calculate the flux reduction observable in the solar cavity compared to the flux postulated to exist in the intergalactic space. A collateral purpose of these calculations is to determine the optimum momentum band to perform antihelium searches with detectors transported by balloons or spacecrafts.

The paper is structured as follows: in Section 2, the simulation code for antihelium interactions with matter is briefly described. In Section 3, the matter thickness of our Galaxy seen by cosmic rays resulting from measurements and calculations is discussed. In Section 4, the antihelium flux reduction caused by the interstellar matter in the Milky Way is calculated in various conditions. In Section 5, an attempt to delimit the form of the $\bar{\alpha}$ rigidity spectra at low energy both in the intergalactic space and in the vicinity of the solar cavity is presented. The attempt is based on conjectures and speculations on the global matter thickness traversed by cosmic antihelium and the effect of the galactic wind. Finally, in Section 6, the conclusions are reported.

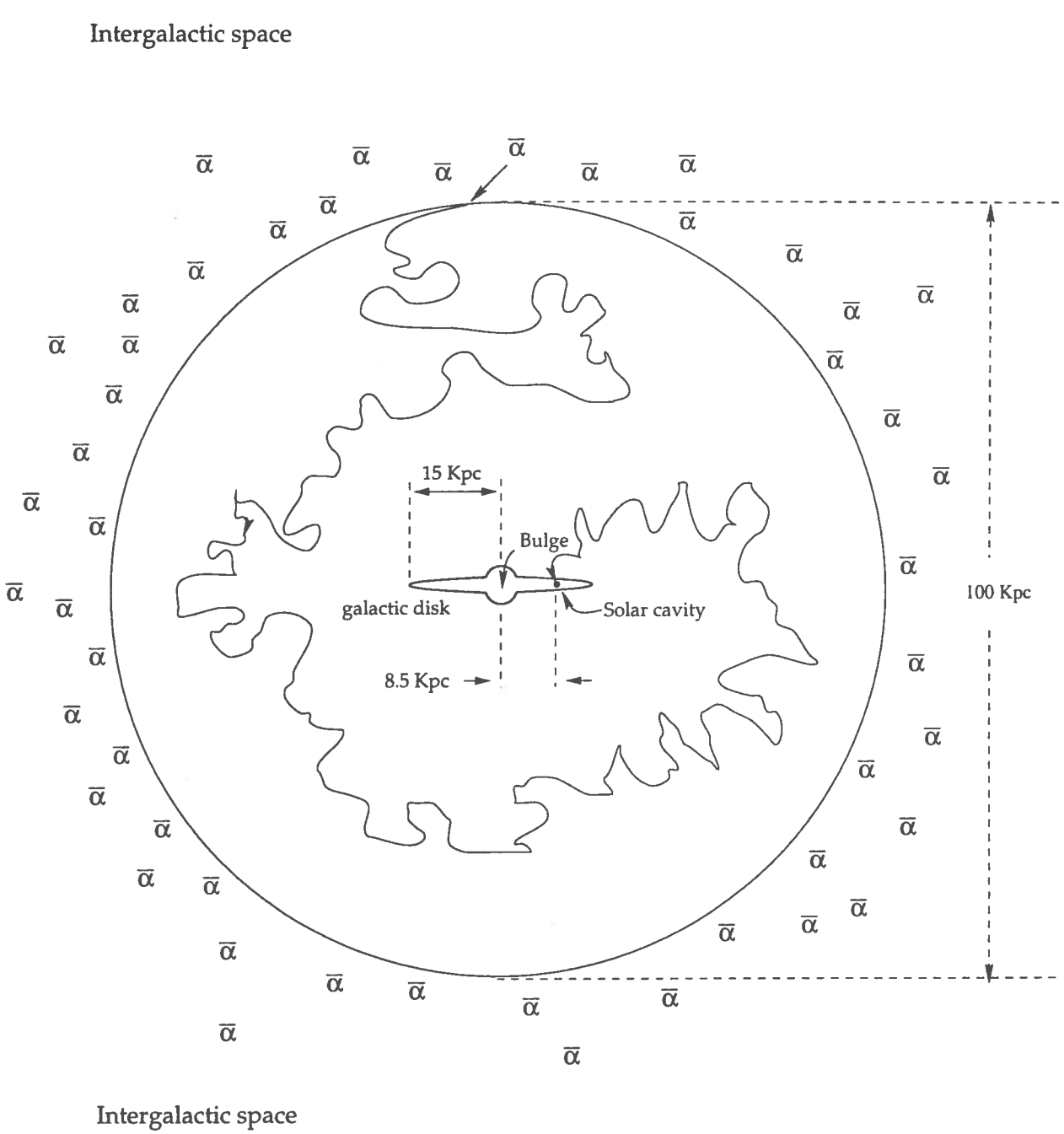

Figure 1: Schematic cross-view of the Galaxy indicating the cosmic antihelium in the intergalactic space, the spherical halo with a diameter of 100 Kpc, the spiral galactic disk and the solar cavity. An antihelium trajectory initiating in the intergalactic space close to the Galaxy, traversing the halo and arriving at the solar cavity is depicted.

2 The simulation code LEASA

The antihelium interactions with interstellar medium have been evaluated by the simulation program called LEASA (Low Energy Antinucleus Simulation Algorithms) developed in the past years (Codino et al. 1989; Brunetti 1991) for the performance evaluation of an apparatus used for antiproton measurements (Hof et al. 1996).

The description of the code LEASA reported in this paper is restricted to those program segments regarding antihelium interactions ($^4\overline{\mathrm{He}}$, $^3\overline{\mathrm{He}}$) and their fragments ($^3\overline{\mathrm{H}}$, $^2\overline{\mathrm{H}}$, $\bar{\mathrm{p}}$, $\bar{\mathrm{n}}$). Those segments of the simulation program irrelevant to these calculations are removed to save computer time. Presently, the code LEASA consists of 24500 Fortran statements.

The parameters of the $\bar{\alpha}$ projectile in LEASA are the initial energy, position and direction. A parallelepiped of external dimensions $10 \times 10 \times 1.1$ km^3 made of 100 equal matter layers of gaseous hydrogen of dimensions $10 \times 10 \times 0.011$ km^3 is appropriate for this calculation, as justified in the beginning of the next Section. The matter thickness encountered by the $\bar{\alpha}$ projectiles is treated as a parameter that may be varied by changing the hydrogen density. The thickness of the hydrogen column swept by cosmic rays is usually referred to as grammage. The external surface of the box is the fiducial volume utilized to signal particle overflow.

The total cross section for the reaction $^4\overline{\mathrm{He}}\,\mathrm{p}$, σ_T, may be split in the two components:

$$\sigma_T = \sigma_E + \sigma_I \tag{1}$$

where σ_I is the inelastic cross section and σ_E is the sum of the elastic and quasi elastic cross sections. We have used a parametrization of the experimental data (Balestra et al. 1985; Balestra et al. 1987a; Balestra et al. 1987b; Balestra et al. 1988) of the reaction $\bar{\mathrm{p}}\,^4\mathrm{He}$ for the cross sections σ_I and σ_E of the reaction $^4\overline{\mathrm{He}}\,\mathrm{p}$. Inelastic interactions of antihelium with interstellar protons are mainly described by two elementary processes:

$$\bar{\mathrm{p}}\mathrm{p} \longrightarrow \text{anything} \tag{2}$$

and

$$\bar{\mathrm{n}}\mathrm{p} \longrightarrow \text{anything} \tag{3}$$

where $\bar{p}$ and $\bar{n}$ are, respectively, the antiproton and antineutron forming the cosmic antihelium and p is the interstellar proton. In table 2, some of the $\bar{p}p$ and $\bar{n}p$ annihilation channels incorporated in the LEASA code are shown. For instance, an important reaction channel is the following:

$$^4\overline{He} + p \longrightarrow (\bar{n}p)_{ann} + {}^3\overline{He} \tag{4}$$

The antineutron-proton pair, $(\bar{n}p)_{ann}$, in the reaction (4) and similar reactions, represents the annihilation between one antineutron of the incident antihelium and a target proton of the interstellar hydrogen, producing secondary hadrons, mainly $\pi^{\pm}$ and π^0.

The cross sections for other channels such as $^4\overline{He}p \rightarrow (\bar{n}p)_{ann}\bar{n}\bar{p}\bar{p}$ and $^4\overline{He}p \rightarrow (\bar{p}p)_{ann}\ \bar{n}\bar{n}\bar{p}$, where in the final state three unbound antinucleons are produced, are modest on the basis of experimental data for the reaction $\bar{p}\,^4He$ at low interaction energy. Note also that break-up reactions of helium e.g. $\bar{p}\,^4He \rightarrow \bar{p}\,n\,^3He$, $\bar{p}\,^4He \rightarrow \bar{p}\,p\,^3H$ and $\bar{p}\,^3He \rightarrow \bar{p}\,p\,d$ have small cross sections in the range of 5 mbarn compared to σ_I of about 280 mbarn in the antiproton momentum interval 500-700 MeV/c, where experimental data are available.

A block diagram illustrating the algorithm for the production of antihelium fragments relevant to this calculation is shown in figure 2. Secondaries emerging from the annihilation vertices are allowed to interact with the ambient matter until they escape from the fiducial volume. Unless experimental data on momenta distribution of secondary particles for specific reaction channels are available, the momenta of secondary particles are assigned by a phase space algorithm available from the CERN libraries.

Ionization energy losses are calculated by the Bethe-Block formula with the appropriate corrections for the absorbing medium. The difference in ionization energy losses between $^4\overline{He}$ and ^4He resulting from the opposite electric charge has been neglected. Antihelium energy losses due to elastic nuclear scattering, ΔT, are given by the following equation:

$$\Delta T = -\frac{t}{2M} \tag{5}$$

where M is the mass of the proton target and t is the 4-momentum transfer squared. The energy losses due to elastic nuclear scattering are calculated by using the small angle approximation, $t \cong -p^2\theta^2$, where p is the particle momentum and θ is the scattering angle in the centre-of-mass system. Antihelium energy losses due to elastic nuclear

Table 2: Reaction channels of the pp, pn, $\bar{p}$p, $\bar{p}$n, π^+p, π^+n, π^-p and π^-n interactions incorporated in the simulation program LEASA

p p interactions	**p n interactions**
$p + p \rightarrow D + \pi^+$	$p + n \rightarrow p + n + \pi^+ + \pi^-$
$p + p \rightarrow p + n + \pi^+$	$p + n \rightarrow 2p + \pi^0 + \pi^-$
$p + p \rightarrow p + n + 2\pi^+ + \pi^-$	$p + n \rightarrow 2p + \pi^-$
$p + p \rightarrow p + p + \pi^+ + \pi^-$	$p + n \rightarrow D + \pi^+ + \pi^-$
$p + p \rightarrow p + p + \pi^0 + \pi^+ + \pi^-$	$p + n \rightarrow D + \pi^0$
$p + p \rightarrow p + p + \pi^0$	$p + n \rightarrow p + n$
$p + p \rightarrow p + p$	
$\bar{p}$ p interactions	**$\bar{p}$ n interactions**
$\bar{p} + p \rightarrow n + \bar{n}$	$\bar{p} + n \rightarrow \pi^+ + 2\pi^-$
$\bar{p} + p \rightarrow \pi^+ + \pi^0 + \pi^-$	$\bar{p} + n \rightarrow \pi^+ + \pi^0 + 2\pi^-$
$\bar{p} + p \rightarrow p + \bar{p} + \pi^+ + \pi^-$	$\bar{p} + n \rightarrow p + \bar{p} + \pi^-$
$\bar{p} + p \rightarrow n + \bar{p} + \pi^+$	$\bar{p} + n \rightarrow 2\pi^+ + \pi^0 + 3\pi^-$
$\bar{p} + p \rightarrow p + \bar{p} + \pi^+ + \pi^- + \pi^0$	$\bar{p} + n \rightarrow 2\pi^+ + 3\pi^-$
$\bar{p} + p \rightarrow p + \bar{p} + \pi^0$	$\bar{p} + n \rightarrow n + \bar{p} + \pi^+ + \pi^-$
$\bar{p} + p \rightarrow 2\pi^+ + 2\pi^- + \pi^0$	$\bar{p} + n \rightarrow \pi^+ + 2\pi^0 + 2\pi^-$
$\bar{p} + p \rightarrow 2\pi^+ + 2\pi^-$	$\bar{p} + n \rightarrow \pi^+ + 3\pi^0 + 2\pi^-$
$\bar{p} + p \rightarrow p + \bar{n} + \pi^-$	$\bar{p} + n \rightarrow 4\pi^0 + 2\pi^-$
$\bar{p} + p \rightarrow \pi^+ + \pi^- + 2\pi^0$	$\bar{p} + n \rightarrow \bar{p} + n$
$\bar{p} + p \rightarrow \pi^+ + \pi^- + 3\pi^0$	
$\bar{p} + p \rightarrow \pi^+ + \pi^- + 4\pi^0$	
$\bar{p} + p \rightarrow 2\pi^+ + 2\pi^0 + 2\pi^-$	
$\bar{p} + p \rightarrow 2\pi^+ + 3\pi^0 + 2\pi^-$	
$\bar{p} + p \rightarrow 2\pi^+ + 4\pi^0 + 2\pi^-$	
$\bar{p} + p \rightarrow 3\pi^+ + \pi^0 + 3\pi^-$	
$\bar{p} + p \rightarrow 3\pi^+ + 2\pi^0 + 3\pi^-$	
$\bar{p} + p \rightarrow 3\pi^+ + 3\pi^0 + 3\pi^-$	
$\bar{p} + p \rightarrow 2\pi^+ + 5\pi^0 + 2\pi^-$	
$\bar{p} + p \rightarrow \bar{p} + p$	
π^+ p interactions	**π^+ n interactions**
$\pi^+ + p \rightarrow \pi^+ + \pi^0 + p$	$\pi^+ + n \rightarrow p + \pi^0$
$\pi^+ + p \rightarrow 2\pi^+ + \pi^0 + \pi^- + p$	$\pi^+ + n \rightarrow p + \pi^+ + \pi^-$
$\pi^+ + p \rightarrow 2\pi^+ + \pi^- + p$	$\pi^+ + n \rightarrow p + 2\pi^0$
$\pi^+ + p \rightarrow n + 2\pi^+$	$\pi^+ + n \rightarrow \pi^+ + \pi^0 + \pi^- + p$
$\pi^+ + p \rightarrow \pi^+ + p$	$\pi^+ + n \rightarrow \pi^+ + n$
π^- p interactions	**π^- n interactions**
$\pi^- + p \rightarrow \pi^- + \pi^+ + n$	$\pi^- + n \rightarrow p + \pi^0 + 2\pi^-$
$\pi^- + p \rightarrow \pi^- + n$	$\pi^- + n \rightarrow p + 2\pi^-$
$\pi^- + p \rightarrow \pi^0 + \pi^- + p$	$\pi^- + n \rightarrow \pi^- + n$
$\pi^- + p \rightarrow \pi^+ + 2\pi^- + p$	
$\pi^- + p \rightarrow n + 2\pi^0$	
$\pi^- + p \rightarrow 2\pi^- + \pi^+ + \pi^0 + p$	
$\pi^- + p \rightarrow \pi^- + p$	

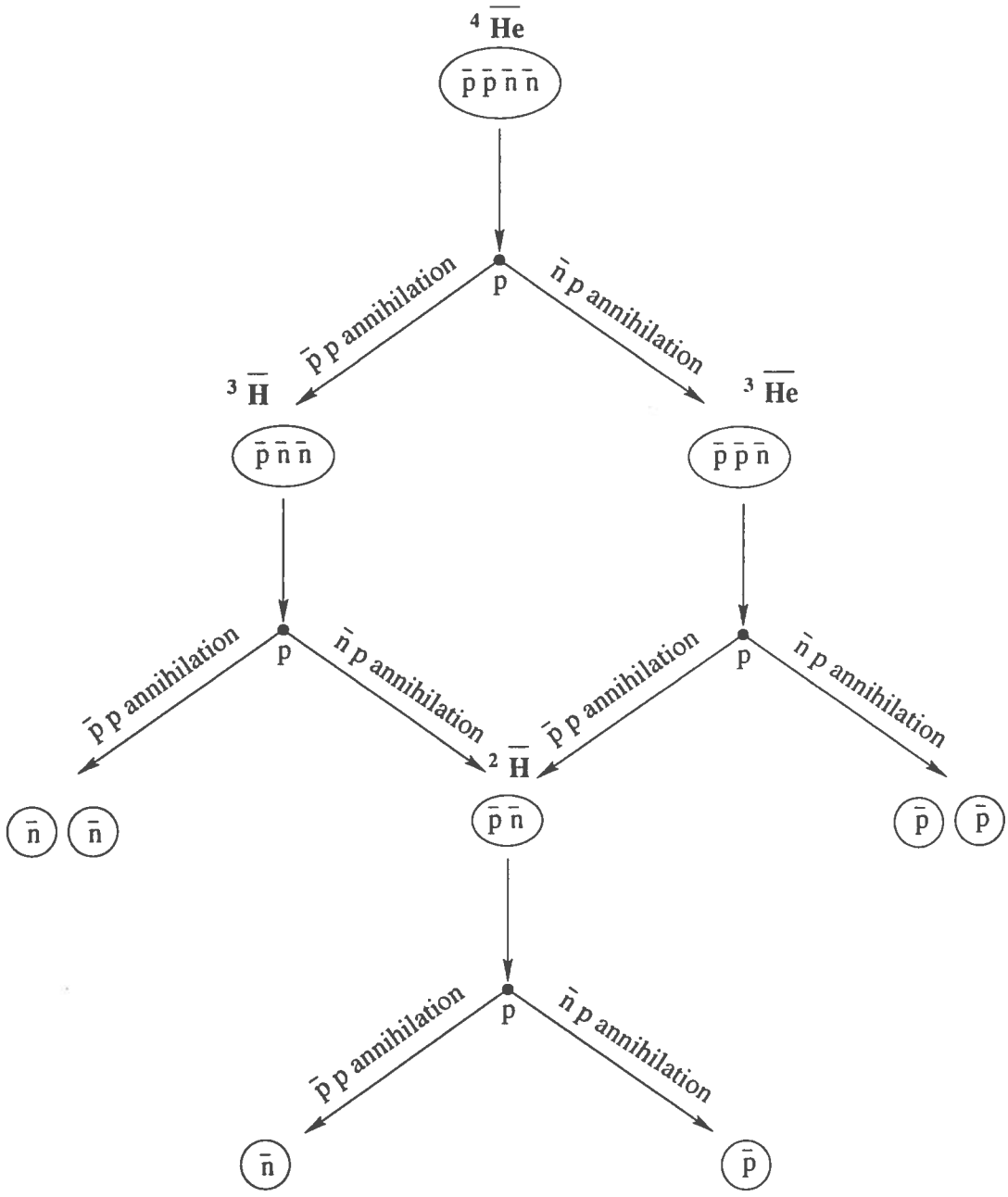

Figure 2: Block diagram indicating the generation of antihelium fragments in LEASA via inelastic collisions of $\bar{\alpha}$ with interstellar protons. According to the experimental data, this mechanism occurs with a probability of 97% at an interaction energy of $s^{1/2}$=4.7 GeV.

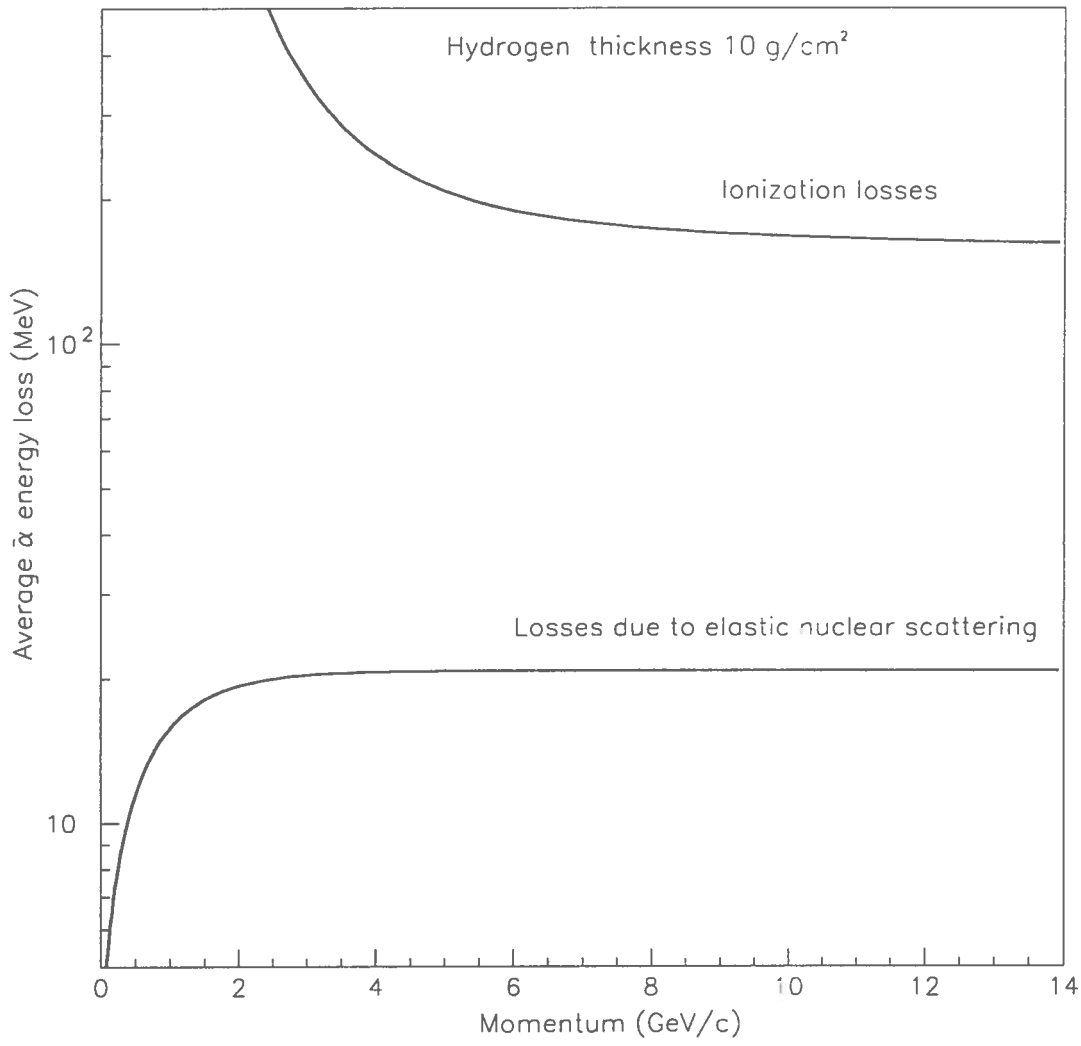

Figure 3: Average energy losses suffered by antihelium in nuclear elastic collisions and by ionization in the interstellar medium as a function of momentum for a matter thickness of 10 g/cm^2.

scattering as a function of momentum are reported in figure 3 for 10 g/cm^2 of hydrogen. For comparison, $\bar{\alpha}$ ionization energy losses are shown in the same figure.

Multiple Coulomb scattering is included in the simulation program. However, its influence on the trajectories and other parameters of cosmic rays is negligible. In fact cosmic rays trajectories, which are deformed helixes (Codino et al. 1995), are determined by the galactic magnetic field which consists of a regular component and a moving random component transported by magnetic clouds.

Two examples of results obtained by the LEASA code are presented in the following. They facilitate the comprehension of the results given in the subsequent sections. In the first example shown in figure 4, the trajectories of the particles generated by an $\bar{\alpha}$ p inelastic interaction occurring in the fiducial volume defined above are described. In the second example, the energy spectra of $\bar{\alpha}$ fragments generated by antihelium of 5 GeV traversing the hydrogen thickness of 10 g/cm^2 have been treated.

A sample of 100000 antialfas has been injected into the matter layers forming the parallelepiped mentioned above. Inelastic collisions occurring in the fiducial volume amount to 63506 events. The rest of the incident $\bar{\alpha}$ sample experienced elastic nuclear scattering and ionization energy losses. Energy spectra are given only for those antinuclides overflowing from the fiducial volume.

The energy spectra of antihelium and its fragments ($^3\overline{\mathrm{He}}$, $^2\overline{\mathrm{H}}$, $\bar{\mathrm{p}}$, $\bar{\mathrm{n}}$) are displayed in figure 5. Note that antitriton and antineutron energy spectra are nearly equal to those of $^3\overline{\mathrm{He}}$ and $\bar{\mathrm{p}}$, respectively. The lower limit of each spectrum is determined by the rest mass of the fragment. The upper limit of the $^3\overline{\mathrm{He}}$ at 3.6 GeV is obtained by the difference between the maximum $^3\overline{\mathrm{He}}$ initial energy (4.1 GeV) and the subsequent average ionization losses of about 500 MeV. Antideuterons are predominantly obtained by $^3\overline{\mathrm{He}}$ inelastic scattering where the $\bar{\mathrm{p}}$p pair annihilates in a reaction similar to that represented by the reaction (4). The peak of the antideuteron energy spectra at about 2.5 GeV results from the difference between the average energy of the parent $^3\overline{\mathrm{He}}$, which is about 3.5 GeV, and the antineutron rest mass lost in the collision. Two different mechanisms shape the antiproton energy spectrum shown in figure 5. The former involves $^3\overline{\mathrm{He}}$ inelastic interaction with the $\bar{\mathrm{n}}$ p annihilation producing in the final state two antiprotons (see figure 2) and the latter inelastic interaction of antideuteron with the $\bar{\mathrm{n}}$ p annihilation producing in the final state one antiproton. The two peakes in the $\bar{\mathrm{p}}$ energy spectrum reflect these production mechanisms.

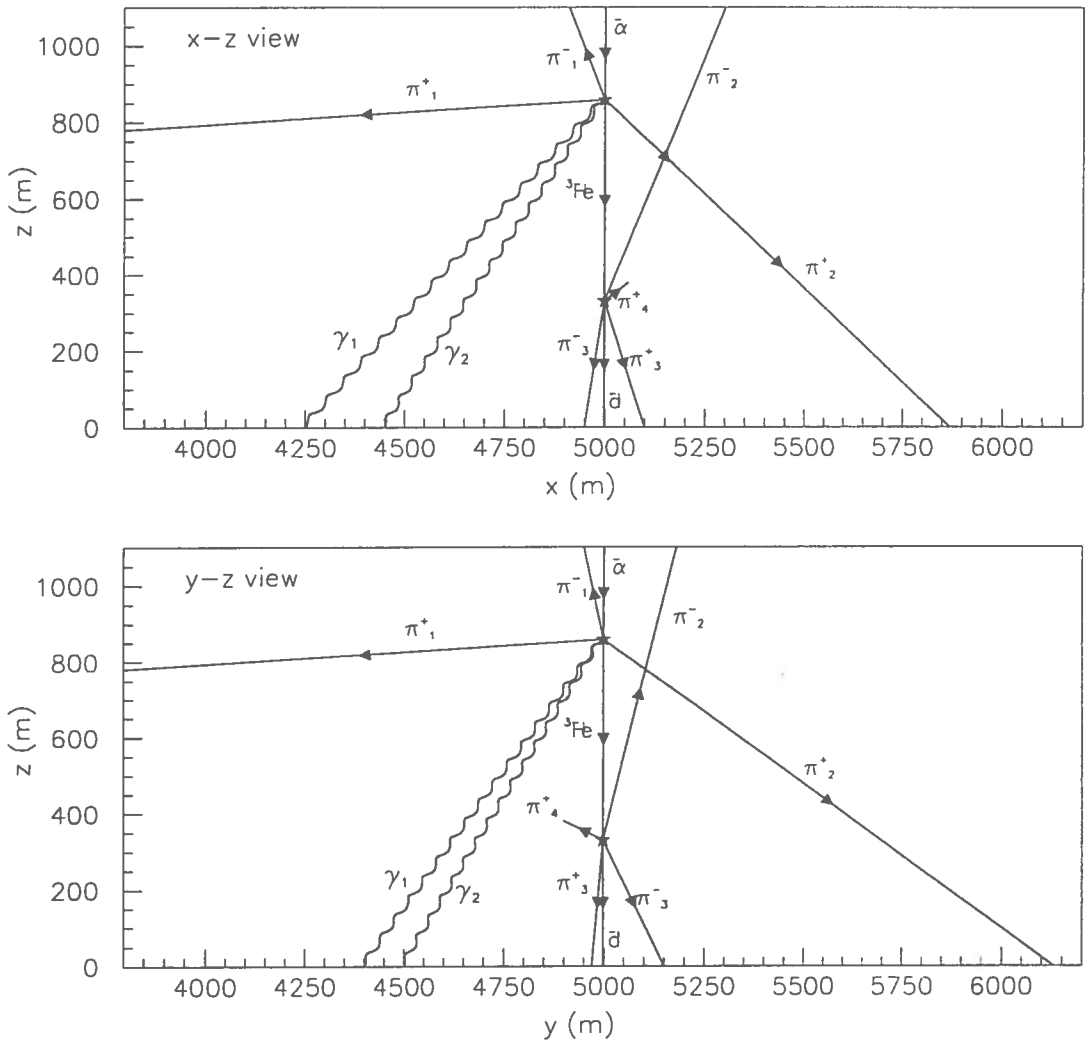

Figure 4: Particle trajectories projected in the $x-z$ and $y-z$ planes of the secondaries emerging from the annihilation vertices of a cosmic $\bar{\alpha}$ of 5 GeV interacting with an interstellar proton. The two black stars represent the annihilation vertices of the primary $\bar{\alpha}$ and $^3\overline{\mathrm{He}}$ fragments. The antideuteron, $\bar{d}$, escaping from the fiducial volume has a kinetic energy of 0.5 GeV.

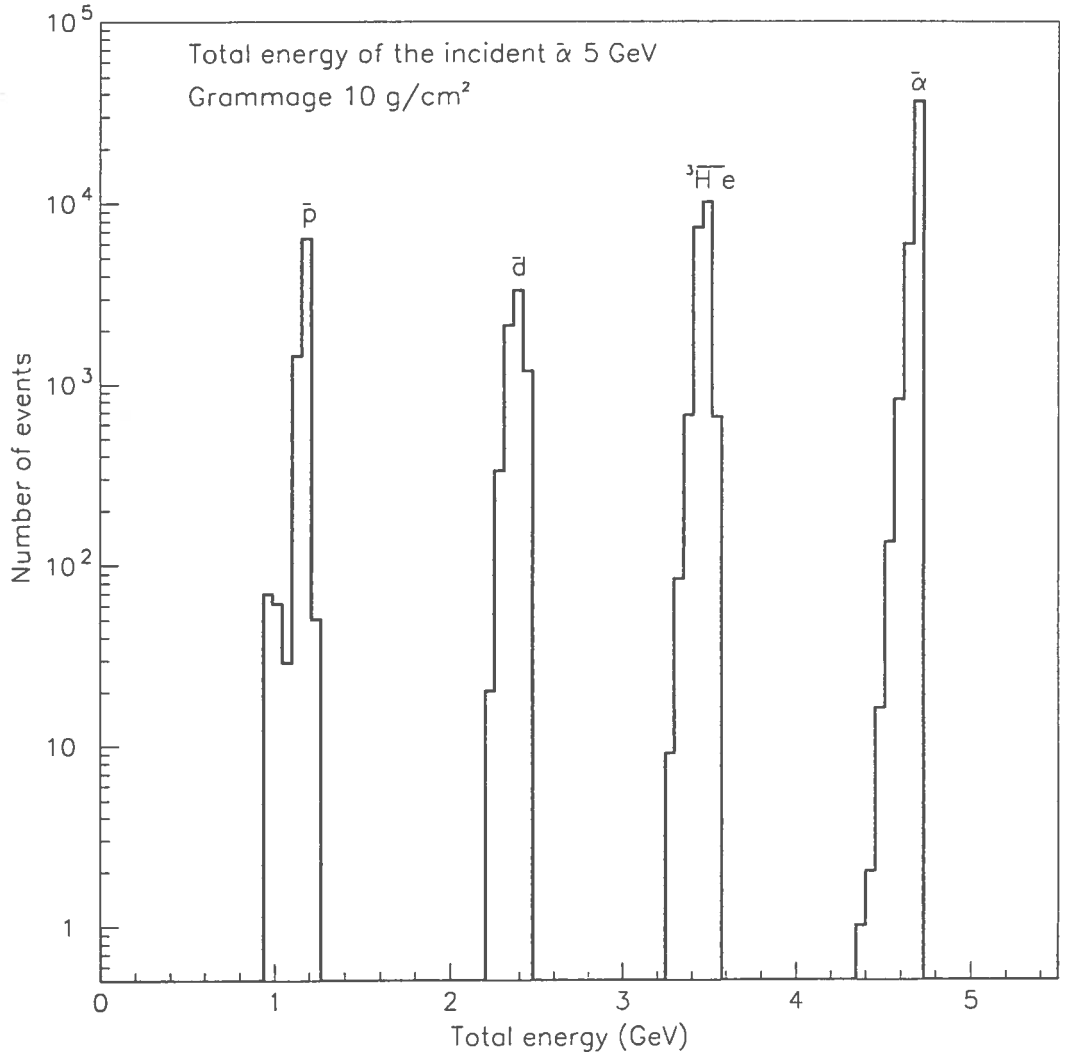

Figure 5: Energy spectra of antihelium and its fragments after the traversal of a matter thickness of 10 g/cm^2 intended to represent the grammage seen by ordinary cosmic rays (nuclides) in the Milky Way.

3 The matter thickness of the Milky Way

In order to accomplish practical calculations, an appropriate schematization of the antihelium interaction processes taking place in the Galaxy is necessary. The description of some measurable properties and effects of cosmic rays in the galactic halo and disk has been made in various versions of leaky box model for the disk and in the diffusion model for the galactic halo (see for instance Stephens 1981; Stecker and Jones 1977 and references therein). For the purpose of these calculations, the most important parameter is, by far, the matter thickness swept by cosmic rays in the Galaxy. The sum of the disk and halo grammages gives the total galactic grammage. Measurements of the energy spectra of spalled nuclei and positrons at low rigidity indicate that cosmic rays traverse on the average a matter column 10 g/cm^2 thick weakly dependent on the rigidity (Webber 1996).

Unfortunately, measurements of the halo grammage have not yet been made though they have been conceived. Thus, the halo thickness, t_h, is estimated by the expression:

$$t_h = m n_h v \tau_h \tag{6}$$

where n_h is the number density of hydrogen in the halo, m is the proton mass, v is the cosmic ray velocity and τ_h is the average confinement time of cosmic rays in the halo. In the diffusion model (Ginzburg and Ptuskin 1976) τ_h is estimated by the following expression:

$$\tau_h = \frac{{L_h}^2}{12D}\left(\frac{8 - 4x^2 + x^3}{2 - x}\right) \cong \frac{{L_h}^2}{3D} \tag{7}$$

where D is the diffusion coefficient, L_d is the half-height of the disk, L_h is the half-height of the confinement region of the halo close to the galactic disk and $x \equiv L_d/L_h$. The values of these parameters are in the following ranges: $100 \leq L_d \leq 150$ pc and $1 \leq L_h \leq 10$ Kpc and D between 3×10^{27} and 10^{29} cm^2 s^{-1}. The values for τ_h are close to 5×10^8 years, which, inserted into the equation (6), give a thickness between 5 and 10 g/cm^2. The number density of hydrogen in the halo is taken to be, on the average, 10^{-2} cm^{-3} (Maffei 1996) with an uncertainty as large as a factor of 10. Therefore, it is likely that the global thickness of the disk and the halo together is between 15 and 20 g/cm^2 for cosmic rays at low energies.

Note that sophisticated algorithms for describing cosmic rays including more accurate spatial boundaries of the disk, the magnetic field configuration and the matter distribution in the galactic volume, though available (Codino et al. 1995), are not necessary for this calculation.

4 Antihelium energy cutoff and flux reduction observable in the solar cavity

High energy antihelium penetrates the galactic cavity and it either makes a nuclear interaction disseminating antiparticle fragments in the Galaxy or it escapes from the halo border populating again the intergalactic space. Relativistic antihelium reaching the galactic disk coming from the intergalactic space without suffering nuclear inelastic interactions loses, on the average, 180 MeV in 10 g/cm^2 of interstellar hydrogen. Low momentum antihelium wanders in the galactic cavity and finally annihilates with the ambient hydrogen. The range - energy relation for antihelium in hydrogen essentially determines this momentum cutoff.

The relative abundances of antihelium fragments produced by inelastic collisions $\bar{\alpha}$ p in the Galaxy as a function of the total grammage is shown in figure 6.

Experiments made by balloon-borne instruments have a residual atmosphere which in most cases may reach the total matter thickness of the Galaxy. Moreover, we cannot fail to mention that the matter thickness of the typical containers shielding the apparatus amounts to several g/cm^2. These circumstances justify the wide range in the matter thickness, from about 10 g/cm^2 to 30 g/cm^2, used for the results of figure 6 and those in the subsequent figures.

It is interesting to determine the fraction of antihelium lost in the galactic cavity as a function of the matter thickness encountered by the extragalactic antihelium. Since the total matter column sensed by cosmic antihelium in the Milky Way is not known with high accuracy, as discussed in the previous section, the fraction of antihelium flux lost in the galactic cavity with different grammages (5, 10 and 15 g/cm^2) has been calculated. It

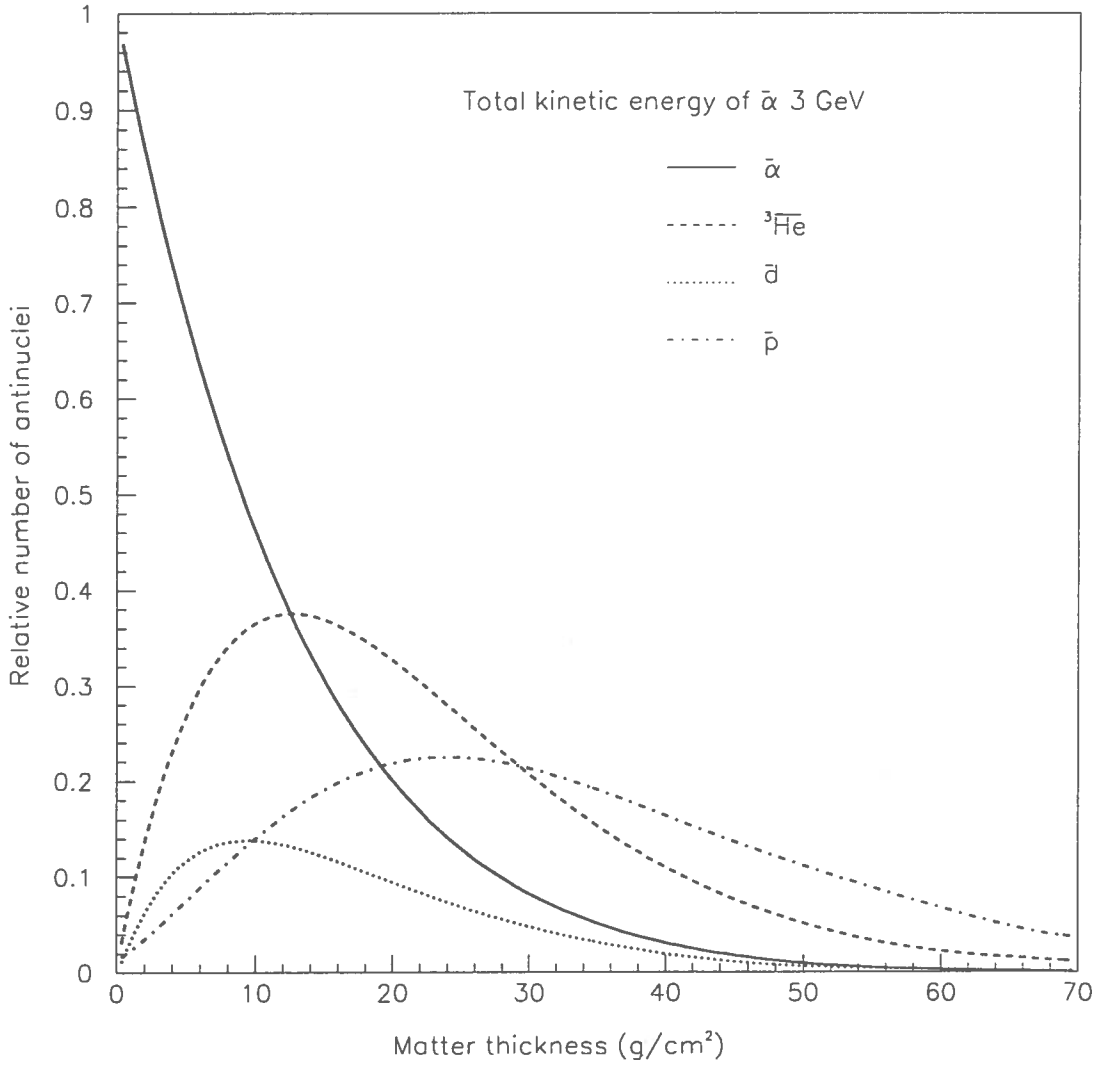

Figure 6: Relative abundances of the antihelium fragments versus matter thickness for inelastic $\bar{\alpha}$ interactions with hydrogen. The annihilation mechanisms described in figure 2 have been utilized in the simulation code LEASA.

is not unreasonable to assume that the effective matter thickness traversed by antihelium ranges between 10 and 15 g/cm^2. The results are shown in figure 7 for antihelium-4. For example, it turns out that no antihelium reaches the solar cavity because of ionization energy losses in the Galaxy for momenta lower than 2 GeV/c and a galactic thickness of at least 6 g/cm^2. The calculations shown in figure 7 indicate that for a specified matter thickness the ionization energy losses and those due to elastic nuclear scattering determine the flux cutoff. For antihelium with momentum greater than 25 GeV/c the flux attenuation which is about 50% for a grammage of 10 g/cm^2 is dominated by the nuclear inelastic cross section. At higher momenta the flux attenuation remains nearly unchanged because the $\bar{\alpha}$p inelastic cross section levels off. The antihelium flux attenuation as a function of the momentum for 3 grammages (5, 10, 15 g/cm^2) is shown in figure 8. For example, the $\bar{\alpha}$ flux is reduced by a factor of 3 at a momentum of 4 GeV/c and a galactic thickness of 15 g/cm^2 with respect to the $\bar{\alpha}$ flux postulated to exist in the intergalactic space. The results in figure 8 can be expressed by the following analytical representation:

$$T(p) = A + Be^{\alpha p} + Ce^{\beta p^2} + De^{\gamma/p} \tag{8}$$

where $T(p)$ is the flux attenuation and p is the $\bar{\alpha}$ momentum. The numerical values of the constants A, B, C, D, α, β, γ are shown in table 3.

Table 3: Numerical values of the constants appearing in the equation (6).

Grammages (g/cm^2)	A	B	C	D	α	β	γ
5	0.46	-0.3	-10	0.3	-0.77	-1.2	-0.8
10	0.02	-0.51	-8	0.55	-0.68	-0.79	-0.5
15	0.006	-3.4	-5	0.43	-1.5	-0.5	-1.18

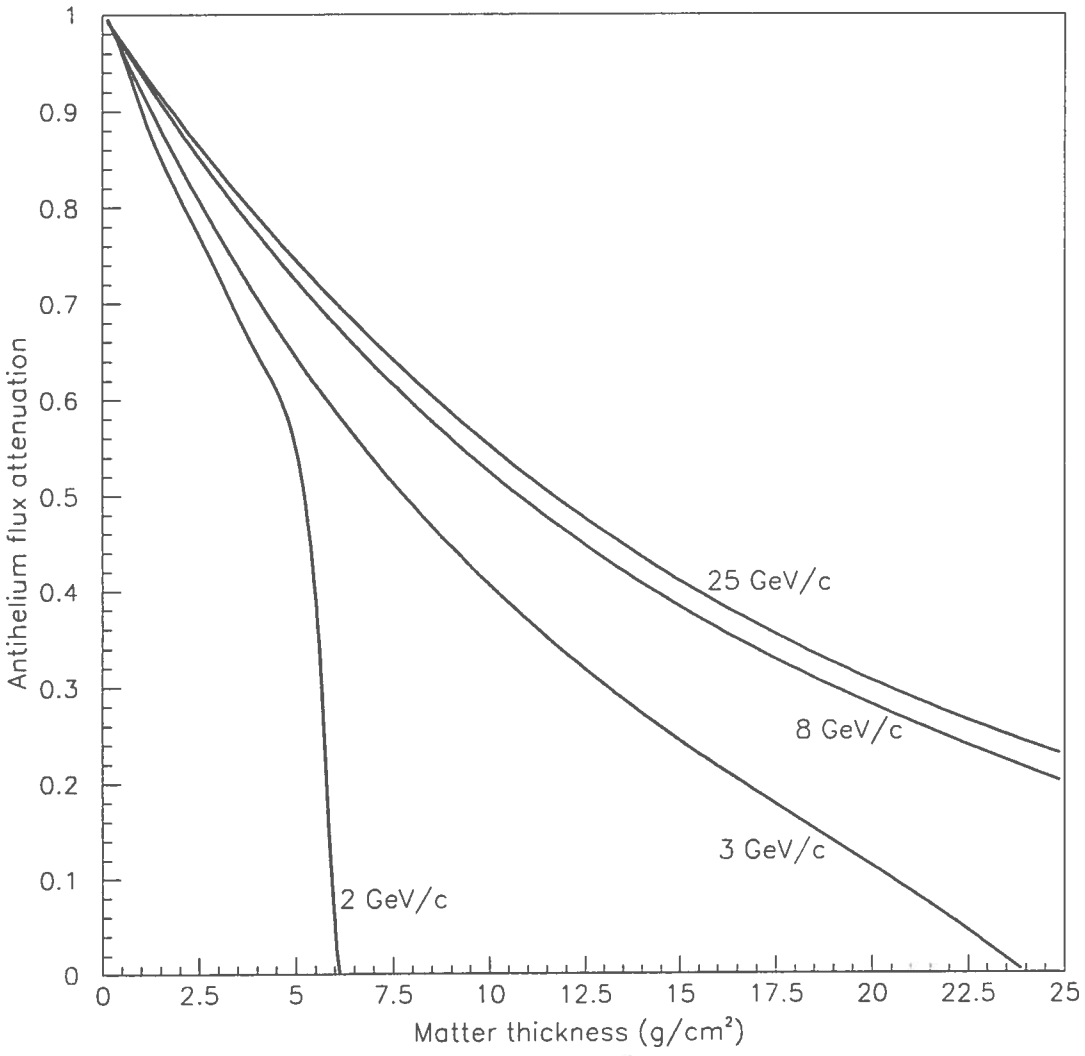

Figure 7: Antihelium flux attenuation observable in the galactic disk plane as a function of the matter thickness (grammages) for various $\bar{\alpha}$ momenta. The antihelium flux has been arbitrarily normalized to 1 in the intergalactic space.

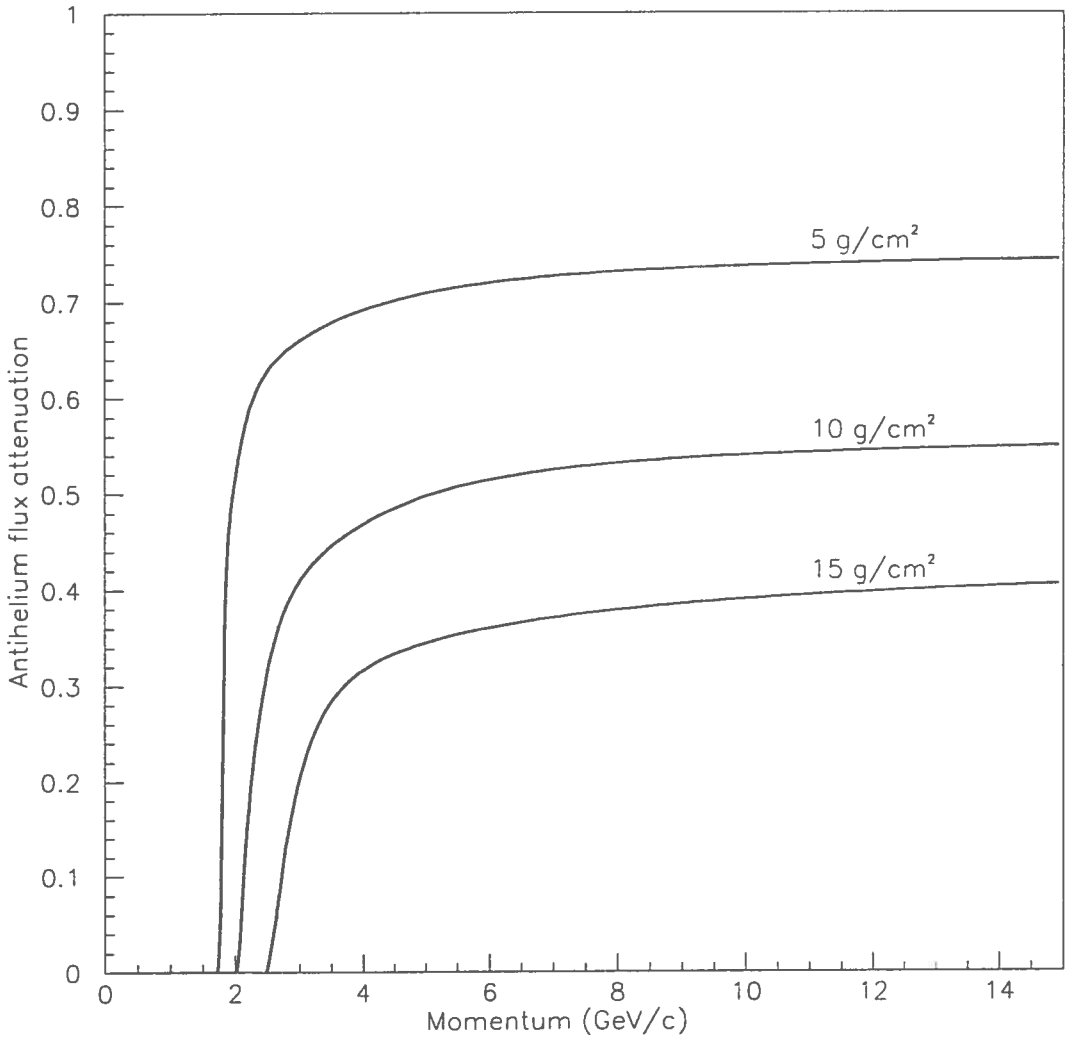

Figure 8: Antihelium flux observable in the galactic disk plane as a function of momentum for various grammages. The antihelium flux has been arbitrarily normalized to 1 in the intergalactic space.

5 Antihelium rigidity spectra

The results on $\bar{\alpha}$ flux attenuation described in the previous section ignore the energy spectrum of intergalactic antihelium. The analytical representation of the $\bar{\alpha}$ flux attenuation given by the function (8) allows one to determine the $\bar{\alpha}$ rigidity spectra, once that of the intergalactic space surrounding our Galaxy is known. However, the flux level and rigidity spectrum of cosmic antihelium in the intergalactic space are totally unknown. In these circumstances, only conjectures may be formulated in order to delimit the range of possibilities for calculating the $\bar{\alpha}$ spectrum. A schematic illustration of the different segments of an antihelium trajectory coming from the parent antigalaxy is displayed in figure 9.

It is well known that there are many types of galaxies: spiral, elliptical, irregular, dwarf and others with various subspecies. For simplicity, we assume in this conjecture that the parent antigalaxy generating cosmic antihelium is a spiral consisting of a disk and a halo with properties (antihydrogen density, magnetic field configuration, stellar populations, etc.) similar to those of the disk and halo of the Milky Way. The $\bar{\alpha}$ trajectory in space regions dominated by antimatter conglomerates may be split into 3 segments associated to the disk, the halo and the intergalactic space. An analogous classification may be adopted for the $\bar{\alpha}$ trajectories in our portion of universe dominated by matter conglomerates, where s_M is the trajectory segment in the intergalactic space s_H is that for the halo, and s_D is that for the disk. The average matter thickness that cosmic rays encounter in each segment of the trajectory is the salient factor in this calculation. The corresponding matter thickness in each segment of the $\bar{\alpha}$ trajectory is denoted by $t_{\bar{D}}$, $t_{\bar{H}}$, $t_{\bar{M}}$, t_M, t_H and t_D. The symmetry between matter and antimatter conglomerates requires $t_{\bar{D}} = t_D$, $t_{\bar{H}} = t_H$ and $t_{\bar{M}} = t_M$. From this reasoning, it follows that the average matter column swept by antihelium arriving in the solar cavity, given by $2t_{\bar{M}} + 2t_{\bar{H}} + 2t_{\bar{D}}$, is about twice that of galactic helium given by $t_D + t_H$. It is likely that $t_{\bar{M}} = t_M \ll t_D + t_H$ because the average hydrogen density inside the galaxies is about 10^5 greater than that in the intergalactic space. These assumptions, based on the postulated symmetric evolution of matter and antimatter conglomerates from microscopic (nuclei and atoms) to macroscopic dimensions (stars, galaxies and filaments), are utilized for the following guess of the $\bar{\alpha}$ energy spectrum, $J(\bar{\alpha})$, observable in the solar cavity.

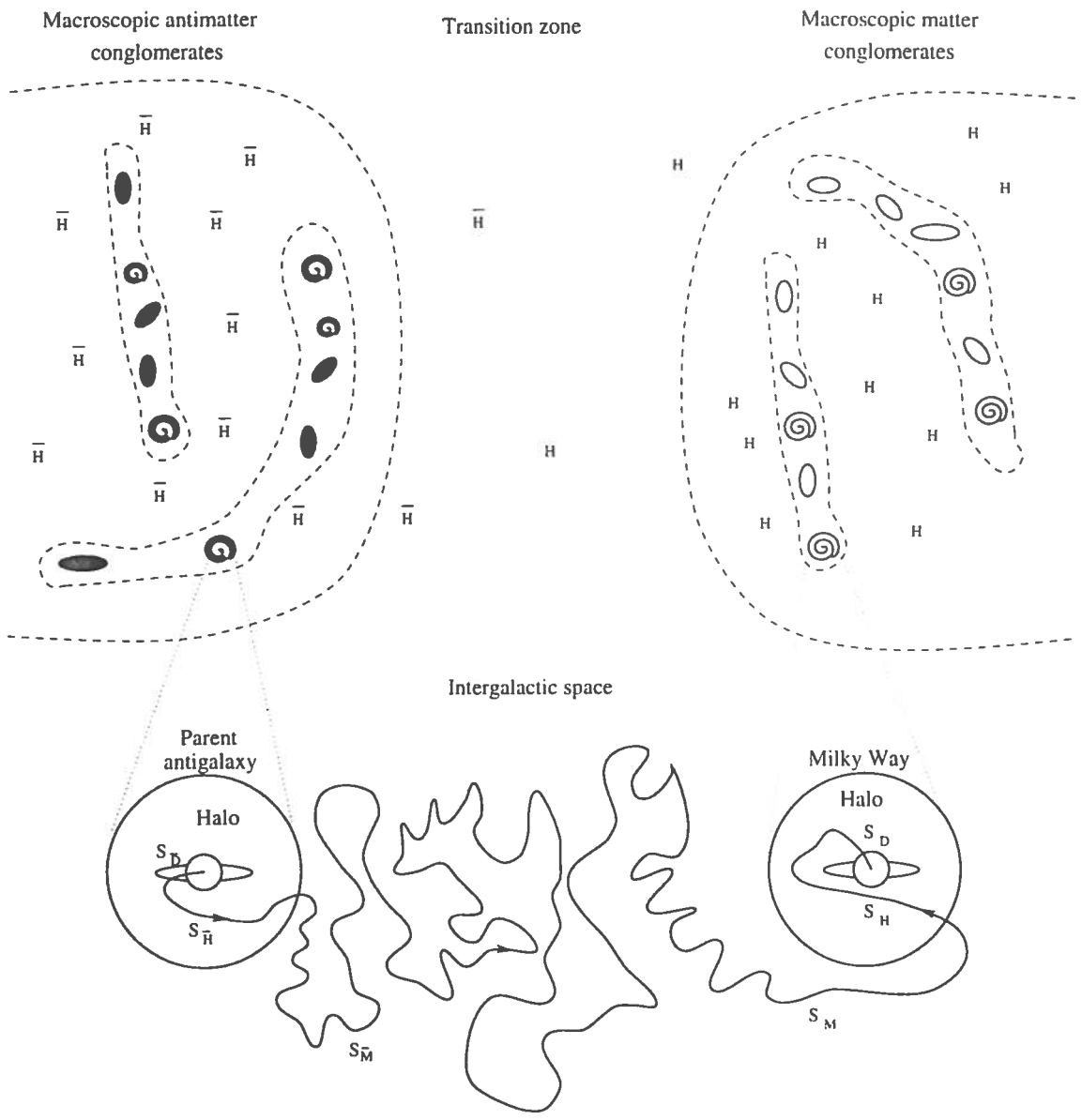

Figure 9: At the top are depicted the matter and antimatter conglomerates separated by a transition zone. The antimatter region includes antihydrogen and antigalaxies arranged in filaments. The matter region is postulated to be structured in a similar way. At the bottom are indicated the different segments ($s_{\bar{M}}$, $s_{\bar{H}}$, $s_{\bar{D}}$, s_M, s_H, and s_D) of an antihelium trajectory coming from a spiral antigalaxy and arriving to the Milky Way, in the following space regions: (1) disk of the antigalaxy ($s_{\bar{D}}$), (2) halo of the antigalaxy ($s_{\bar{H}}$), (3) intergalactic space in antimatter conglomerates ($s_{\bar{M}}$). (4) intergalactic space in matter conglomerates (s_M), (5) halo of Milky Way (s_H), (6) local galactic disk (s_D).

The helium energy spectrum at the top of the atmosphere produced in our Galaxy has been measured by many experiments in the energy range 100 MeV up to 200 GeV. It may be represented by the power law expression:

$$J(\alpha) = AE^{-\gamma} \qquad E \geq 3\text{GeV/u} \tag{9}$$

where $A = 500$ particles/m^2 s sr (GeV/u)$^{1-\gamma}$ and the spectral index, γ, equals to 2.70±0.03. In the low energy range, E≤0.2 GeV/u, the spectrum may be approximated by the relation:

$$J(\alpha) = BE^{\beta} \qquad E \leq 0.2\text{GeV/u} \tag{10}$$

where $B = 2510$ particles/m^2 s sr (GeV/u)$^{1-\gamma}$ and $\beta = 0.03$.

The antihelium energy spectrum in the antigalaxy is postulated to be equal to that of helium observed in our Galaxy and is represented by the equations (9) and (10). Thus, we postulate, together with Ahlen et al. 1982, $J(\bar{\alpha}) = J(\alpha)$ in the parent antigalaxy. The $\bar{\alpha}$ energy spectrum is modified by nuclear and electromagnetic interactions with ambient matter during the voyage from the source to the proximity of the solar cavity. The resulting $\bar{\alpha}$ energy spectra in the intergalactic space (dashed lines) surrounding the Milky Way are shown in figure 10. The intensity of the $\bar{\alpha}$ spectrum close to the intergalactic space surrounding the Milky Way is determined by the distance, power of cosmic ray sources and other parameters of the antimatter conglomerates. On the other hand, the shape is mainly determined by the physical processes described in section 3. Following the experimental data of table 1, it is plausible to envisage that at least 6 orders of magnitude separate the helium and antihelium rigidity spectra in the proximity of the solar cavity. The differences between the $\bar{\alpha}$ and α momentum spectra shown in figure 10 point out that the expected $\bar{\alpha}/\alpha$ ratio versus momentum reaches a maximum value and then remains constant only beyond a certain momentum for a specified grammage. For example, the $\bar{\alpha}/\alpha$ ratio is 0.39 for momenta greater than 15 GeV/c and a grammage of 15 g/cm^2.

The number of $\bar{\alpha}$, $N(\bar{\alpha})$, with momenta greater than a specified value, p_{min}, has been computed from the curves shown in figures 10 and 8 by the expression:

$$N(\bar{\alpha}) = C \int_{p_{min}}^{+\infty} J(\bar{\alpha})\, dp \tag{11}$$

where $J(\bar{\alpha})$ is the momentum spectrum of $\bar{\alpha}$ displayed in figure 10, and C is a constant related to the experiment which takes into account the observing time, the geometrical

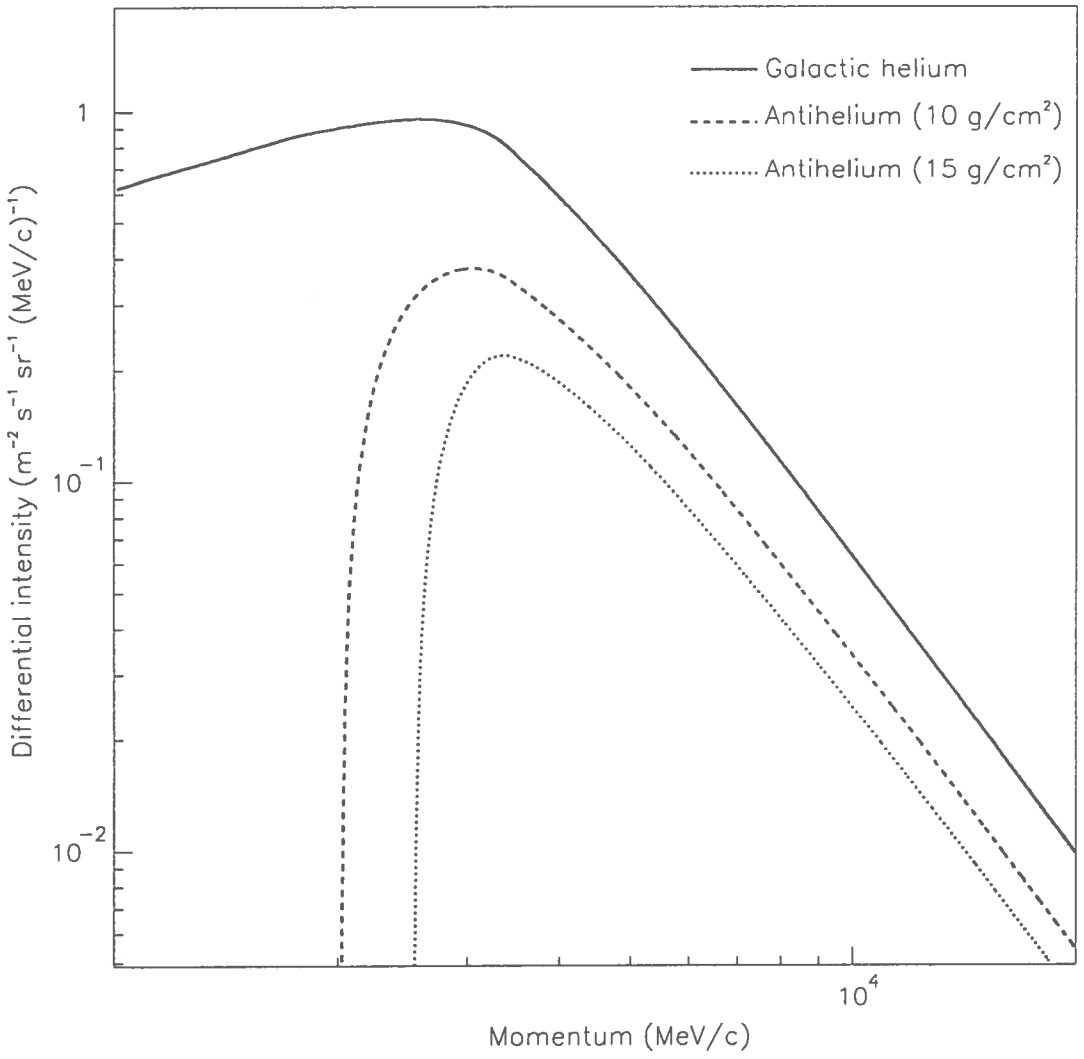

Figure 10: Helium momentum spectrum in the interstellar space of our Galaxy (solid line). Antihelium momentum spectrum observable in the solar cavity (dashed and dotted lines). The $\bar{\alpha}$ spectrum in the parent antigalaxy has been arbitrarily normalized to that of helium observed in the interstellar medium of our Galaxy. The normalization of the $\bar{\alpha}$ flux to that of helium in the Milky Way is discussed in the text.

factor, the α and $\bar{\alpha}$ detection efficiencies and similar empirical parameters of the instrument. In the subsequent results, we put $C = 1$. The number of helium events, $N(\alpha)$, is computed in a similar way. The computed ratio $N(\bar{\alpha})/N(\alpha)$ versus p_{min} for the 3 grammages of 10, 20 and 30 g/cm^2 is shown in figure 11.

An additional, severe attenuation of the $\bar{\alpha}$ flux is caused by the galactic wind. The $\bar{\alpha}$ rigidity spectra $J(\bar{\alpha})$ shown in figure 10 are modified by the effect of the galactic wind. An interesting discussion of the existence of the galactic wind and its parametrization may be found in Ahlen et al. 1982. The modified $\bar{\alpha}$ momentum spectra due to the galactic wind parametrized by the formula of Ahlen et al 1982. are displayed in figure 12 for 3 different grammages. The computed ratio $N(\bar{\alpha})/N(\alpha)$ versus p_{min} for the three different grammages of 10, 15 and 30 g/cm^2 is shown in figure 13. The effect of the galactic wind on the $\bar{\alpha}$ rigidity spectra described in figure 12 is incorporated in this result.

6 Conclusions

Speculations derived from symmetric theories of the Universe suggest that cosmic antinuclei might populate the intergalactic space. Following this speculation, we have assumed that a finite flux of cosmic antihelium is present in the intergalactic space surrounding the halo of the Milky Way, as pictorially illustrated in figure 1.

The calculations presented in this paper demonstrate that there is a cutoff at low rigidity in the antihelium flux observable in the solar cavity. The cutoff value is determined by the matter column thickness encountered by the antihelium while travelling from the halo to the disk of our Galaxy. The flux attenuation for 3 grammages as a function of the antihelium momentum are reported in figure 8.

The critical importance of the results shown in figure 8 related to experiments searching for cosmic antihelium is vividly illustrated by the following example. Suppose that two different experiments, denoted by A and B, have determined the same upper limit to the $\bar{\alpha}/\alpha$ flux ratio with the same confidence level of 95% in two different momentum

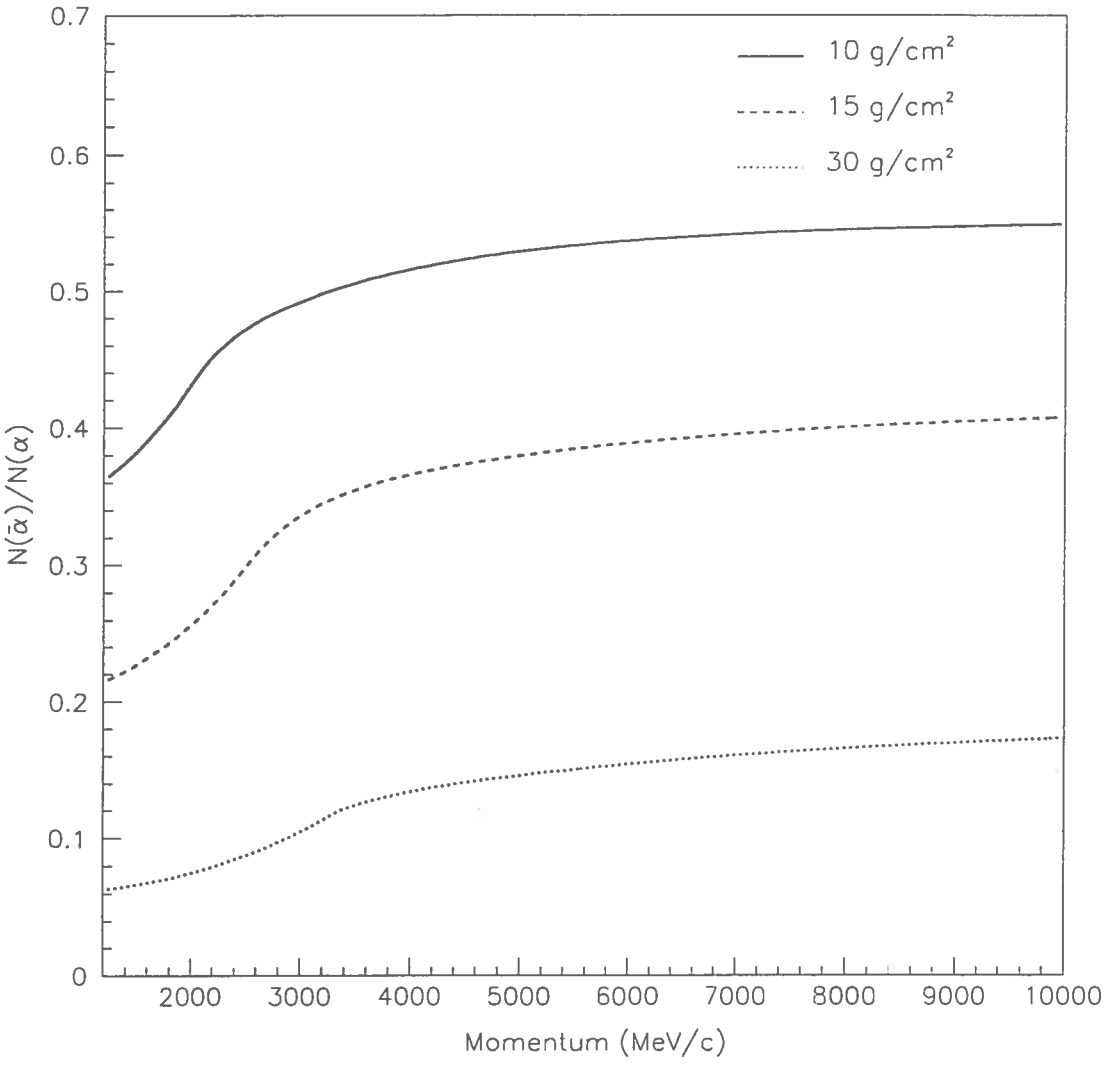

Figure 11: Computed ratio of the number of antihelium-to-helium events as a function of the momentum. The $N(\bar{\alpha})/N(\alpha)$ ratio at a given momentum, p, is calculated by taking all the α and $\bar{\alpha}$ events having momenta greater than p.

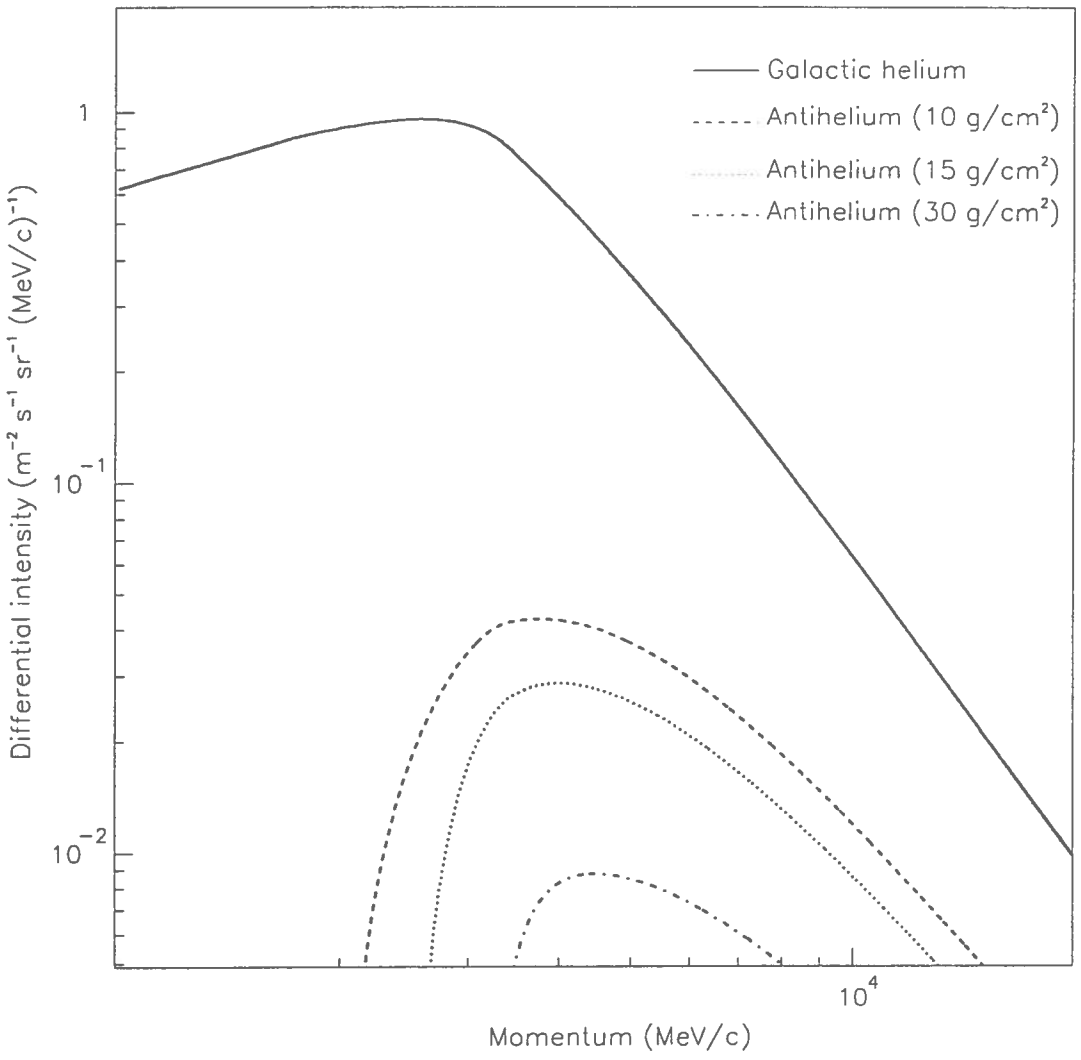

Figure 12: Helium momentum spectrum in the interstellar space of our Galaxy (solid line). Antihelium momentum spectra shaped by the galactic wind obtained by applying the parametrization reported in in Ahlen et al. to the original momentum spectra shown in figure 10 (dashed and dotted lines). The normalization of the $\bar{\alpha}$ flux to that of helium in the Milky Way is discussed in the text.

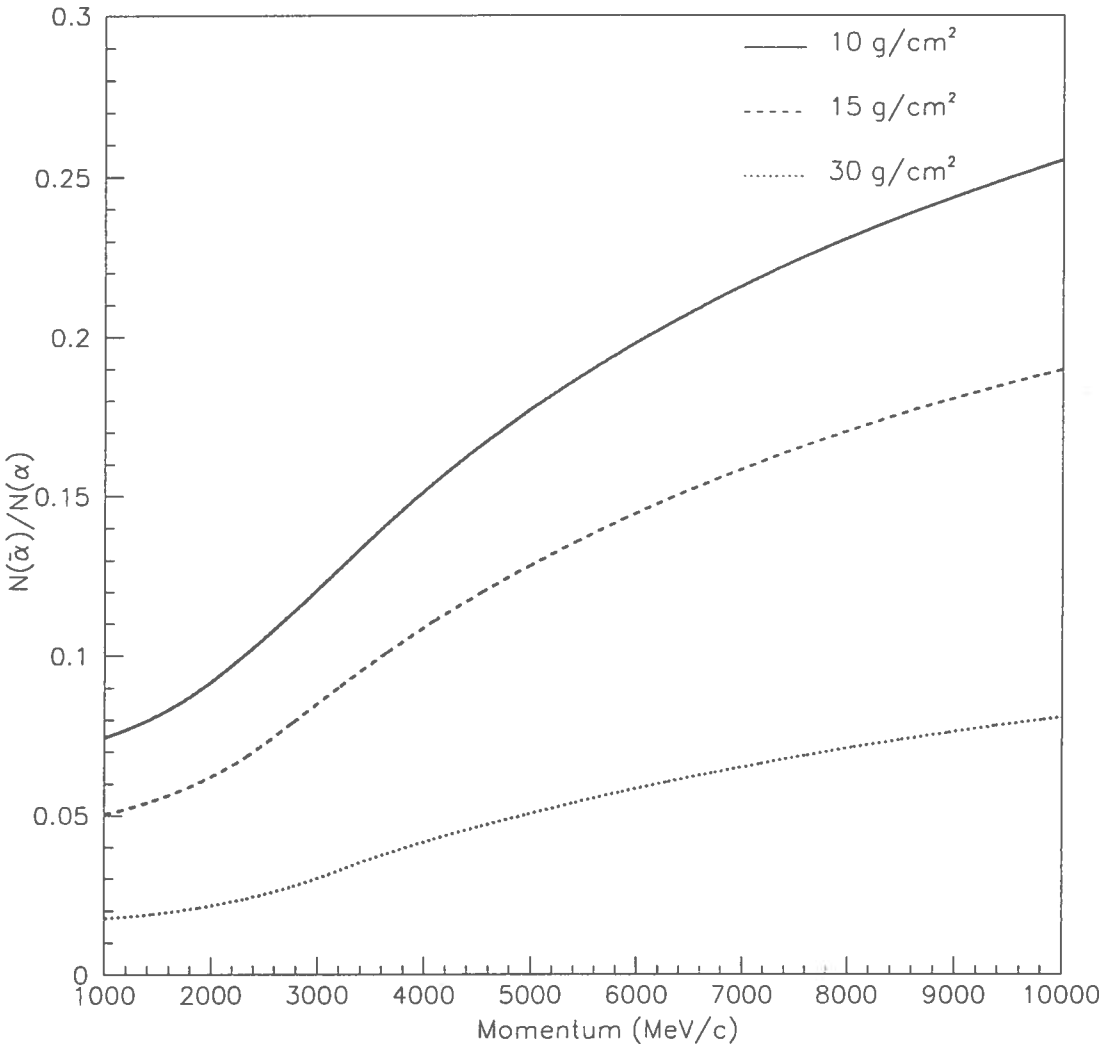

Figure 13: Computed ratio of the number of antihelium-to-helium events as a function of the momentum. The $N(\bar{\alpha})/N(\alpha)$ ratio at a given momentum, p, is calculated by taking all the α and $\bar{\alpha}$ events having momenta greater than p with the effect of the galactic wind.

bands. The experiment A collected events with momenta greater than 2 GeV/c and the experiment B with momenta greater than 10 GeV/c. From the curves of figure 11 the $N(\bar{\alpha})/N(\alpha)$ ratio is 0.062 ($y_A = 0.062$) for the experiment A and 0.19 ($y_B = 0.19$) for the experiment B. A grammage of 15 g/cm^2 has been assumed in both experiments. As a consequence, the upper limit to the $\bar{\alpha}/\alpha$ flux ratio or the sensitivity of the experiment A is reduced by a factor $y_B/y_A = 3$ compared to experiment B.

Historically, the most sensitive antialfa searches (Buffington et al. 1981; Ormes et al. 1995) have been accomplished at low rigidity (see table 1) where the ordinary cosmic ray flux is at its highest level. In this paper, we have demonstrated that the antihelium flux in the galactic cavity is expected to be negligible in the low momentum band. The upper limits to the antinucleus-to-nucleus flux ratios of table 1 may be, in principle, corrected taking into account the results reported in this paper. However, quantitative corrections may be only done including in the evaluation the specific experimental conditions of the data taking (geomagnetic cutoff, solar modulation, residual atmospheric thickness in ballon-borne instruments and other parameters).

Note that no mention has been done of the critical importance of the $\bar{\alpha}$ flux depression at low momenta in those experiments giving upper limits to the $\bar{\alpha}/\alpha$ ratio as reported in table 1.

Future experiments searching for antinuclei should explore high rigidity intervals in the range of tens of GV/c. The optimum rigidity range for the quest of cosmic antihelium is located beyond 5 GV/c as obtained from this calculation which utilizes as a major parameter a galactic thickness delimited by observational data.

Aknowledgments

We express our gratitude to A. W. Wolfendale for useful discussions during the Vulcano Workshop (1996) regarding the spatial extension and intensity of the magnetic field in the galactic halo which affects the global grammage encountered by extragalactic cosmic rays arriving at the galactic disk.

We wish to thank Prof. Paolo Maffei of University of Perugia, Italy, for useful discussions on the techniques for measuring the hydrogen density in the galactic halo.

We are greatful to S. A. Stephens of Tata Institute of Bombay (India) for enlightening remarks during the initial stage of this work on the galactic wind effects on extragalactic cosmic rays.

References

Ahlen S. P. et al. 1982, the The Astrophysical Journal, **260**, 20.

Aizu H. et al. 1961, Physical Review, **121**, 1206.

Badhwar G. D. et al. 1978, Nature, **274**, 137.

Balebanov V. M. et al. 1995, AMS technical proposal, unpublished.

Balestra F. et al. 1985, Phys. Lett. **165B**, 265.

Balestra F. et al. 1987a, Nucl. Phys. **A465**, 714.

Balestra F. et al. 1987b, Phys. Lett. **194B**, 343.

Balestra F. et al. 1988, Phys. Lett. **215B**, 247.

Brunetti M. T. 1991, "Rivelazione di antielio cosmico in un calorimetro al silicio", Thesis, University of Perugia, Italy.

Buffington A. et al. 1981, The Astrophysical Journal, **248**, 1179.

Codino A. et al. 1989, Il Nuovo Cimento, **103B**, 319-331.

Codino A. et al. 1994, Astrophysics and Space Science, **220**, 131.

Codino A. et al. 1995, Proceedings of the XXIV ICRC Rome, **Vol. 3**, page 100.

Evenson P. et al. 1972, The Astrophysical Journal, **176**, 797.

Ginzburg V. L. and Ptuskin V. S. 1976, Review of Modern Physics, **48**, 161.

Golden R. L. et al. 1974, The Astrophysical Journal, **192**, 747.

Greenhil J. G. et al. 1971, Nature, **230**, 170.

Grigorov N. L. et al. 1964, Soviet Phys. JETP, **18**, 272.

Hof M. et al. 1995, The Astrophysical Journal, **467**, L33.

Ivanova N. S. et al. 1968, Cosmic Res., **66**, 69.

Lund N. and Rotenberg M. 1986, Astronomy and Astrophysics, **164**, 231-236.

Maffei P. 1996, private communication.

Ormes J. F. et al. 1995, Proceedings of the XXIV ICRC Rome **Vol. 3**, page 92.

Smoot G. F. et al. 1975, Phys. Rev. Letters, **35**, 258.

Stecker F. W. and Jones F. C. 1977, the The Astrophysical Journal, **217**, 843-858.

Stephens S. A. 1981, Nature **289**, 267-269.

Verma R. P. et al. 1973, Nature Physical Science, **240**, 105.

Webber W. R. 1995, The Astrophysical Journal, **457**, 435.